

See discussions, stats, and author profiles for this publication at: <https://www.researchgate.net/publication/271714215>

Silver Oxide as Superb and Stable Photocatalyst under Visible and Near-Infrared Light Irradiation and Its Photocatalytic Mechanism

ARTICLE in INDUSTRIAL & ENGINEERING CHEMISTRY RESEARCH · JANUARY 2015

Impact Factor: 2.59 · DOI: 10.1021/ie503241k

CITATIONS

4

READS

31

7 AUTHORS, INCLUDING:



Wei Jiang

Sichuan University

22 PUBLICATIONS 145 CITATIONS

[SEE PROFILE](#)



Shaojun Yuan

Sichuan University

56 PUBLICATIONS 1,062 CITATIONS

[SEE PROFILE](#)



Houfang Lu

Sichuan University

28 PUBLICATIONS 549 CITATIONS

[SEE PROFILE](#)

Silver Oxide as Superb and Stable Photocatalyst under Visible and Near-Infrared Light Irradiation and Its Photocatalytic Mechanism

Wei Jiang,* Xiaoyan Wang, Zhaomei Wu, Xiaoning Yue, Shaojun Yuan, Houfang Lu, and Bin Liang

Multi-Phases Mass Transfer and Reaction Engineering Laboratory, College of Chemical Engineering, Sichuan University, Chengdu 610065, China

Supporting Information

ABSTRACT: Photocatalytic processes are an environmentally friendly technology for treatment of persistent organic pollutants. However, the majority of current photocatalysts cannot utilize sunlight sufficiently to realize fast decomposition of organic pollutants. In this research, a silver oxide nanoparticle aggregation with superb photocatalytic performance under artificial light source and sunlight was prepared and characterized. The results showed that methyl orange (MO) was decomposed completely in 120 s under irradiation of artificial visible light, artificial ultraviolet light, and sunlight, and in 40 min under near-infrared (NIR) light. The superb photocatalytic performance of as-prepared silver oxide remained almost constant after reuse or exposure under sunlight. It was confirmed that the co-working effect of photogenerated hole and ozone anion radicals did play an important role in the process of MO photodegradation with the existence of Ag_2O . The narrow band gap of Ag_2O , less than 1.3 eV, resulted in the photocatalytic performance of Ag_2O under NIR light. Furthermore, the high surface area and numerous crystal boundaries provided by the aggregation of Ag_2O nanoparticles efficiently increased the escape probability of photogenerated electrons and the contact probability of photogenerated holes with outside materials, assuring superb photocatalytic activity and excellent stability of as-prepared Ag_2O samples.

1. INTRODUCTION

Semiconductor photocatalysts remain an area of intense research focus for utilization of solar energy, and one of the major important applications investigated in photocatalysis technology is color removal and destruction of persistent organic pollutants, especially dyes that constitute the largest group of hazardous organic compounds and represent an increasing environmental danger.^{1–13} The TiO_2 photocatalyst has attracted great attention because of powerful decomposition ability, ambient operating conditions, low cost, and environmental friendliness since it was first used for water photolysis.^{2–8} However, the cost competitiveness of TiO_2 photocatalysis processes is still inferior owing to the low quantum efficiency and narrow available spectrum. Higher performance of the photocatalysis process can be achieved by either enhancing the quantum efficiency of photocatalysis under ultraviolet (UV) light, introducing visible light activity that is absent with pure TiO_2 , or seeking new photocatalytic materials with novel composition and structure.⁹ From a practical point of view, alternative photocatalytic materials that are as versatile, economical, stable, abundant, and non-toxic as TiO_2 are the desired goal.

Investigation is mainly focused on new photocatalysts with higher photocatalytic performance, better stability, and wider available light spectrum.^{14–17} However, successful improvement in all three aspects simultaneously is rarely reported. N-doped TiO_2 , BiVO_3 , etc., are stable, but their reaction time is more than 30 min.^{18–22} Silver salts exhibit superb visible light-response photocatalytic activation to organic dye in 10–15 min, but are easy to decompose and exhibit no response to near-infrared (NIR) light.^{23–30} $\text{YF}_3\text{-Yb}^{3+}\text{-Tm}^{3+}/\text{TiO}_2$ and $\text{Cu}_2(\text{OH})_3\text{Cl}$

PO_4 can work under NIR irradiation, but the reaction time is far longer than 6 h.^{31,32}

Recently, notable progress in the photocatalysis process is the observation of silver-containing photocatalysts, such as Ag_3PO_4 , Ag_3VO_4 , and Ag_2CO_3 , which exhibit excellent photocatalytic activity in degrading persistent organic pollutant in contrast to the other visible light driven photocatalysts such as N-TiO_2 , BiVO_3 , Zn_2S . The target organic dyes such as methyl blue, rhodamine, and methyl orange (MO), can be decomposed in 10–15 min. However, the above silver oxyacid salts will be easily photodecomposed under light irradiation, generating metallic silver. Consequently, their photocatalytic performance decreases sharply. This property of silver oxyacid salts does not augur well for its future application. Besides, the limitation of the band gap of silver oxyacid salts (i.e., Ag_3PO_4 , 2.36 eV; Ag_3VO_4 , 2.06 eV; Ag_2CO_3 , 2.30 eV^{23,26,27}) results in the exclusive usage of UV and visible light. Because red/NIR radiation (650–1000 nm) accounts for approximately 33% of the solar energy arriving at the surface of the earth, while UV-visible (UV-vis) radiation (350–650 nm) accounts for about 40%,³³ the key issue toward achieving higher efficiency of photocatalyst is in the development of red and NIR absorbing photocatalytic materials to utilize more of the solar spectrum.

Ag_2O , a brown powder possessing a simple cubic structure with a lattice parameter of 0.472 nm, was rarely employed as a candidate for visible light driven photocatalyst although its corresponding oxyacid salts have been investigated widely.

Received: August 18, 2014

Revised: October 27, 2014

Accepted: December 24, 2014

Published: December 26, 2014

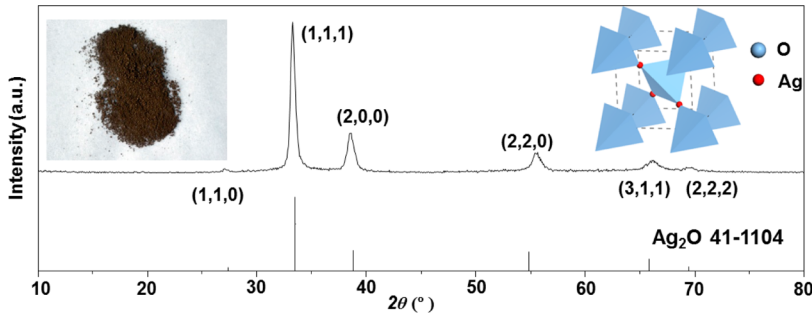


Figure 1. Appearance, XRD pattern, and crystal structure of fresh Ag_2O sample.

There were two attempts to adopt Ag_2O as photocatalyst under visible light irradiation. Wang et al.³⁴ introduced Ag_2O to decompose MO, and its activity can remain almost unchanged after five cycles with relatively long degradation time of 160 min. $\text{Ag}@\text{Ag}_2\text{O}$ photocatalysts³⁵ were fabricated and exhibited high efficiency, which decomposed MO in 10 min under visible light irradiation. This confirms that Ag_2O is a potential photocatalyst simultaneously possessing excellent performance and high stability. It is highly interesting and a great challenge to explore such new and efficient silver oxide photocatalytic materials that are sensitive to a spectrum wider than that of traditional photocatalyst, containing UV, visible, and red/NIR light, with good stability and superb photocatalytic activity.

We report a new use of Ag_2O semiconductor, which exhibits fast photocatalytic performance to methyl orange and excellent stability under visible and near-infrared light. It displays a high utilization rate of solar energy and potential practicability for environmental protection.

2. EXPERIMENTAL SECTION

2.1. Preparation of Ag_2O . All analytical grade reagents, including AgNO_3 , H_3BO_3 , NaOH , methyl orange, *tert*-butanol, indigo carmine, and 1,4-benzoquinone, were purchased from ChengDu Kelong Chemical Reagent Co. Ltd. and used directly without further purification.

Powder samples were prepared by the ion-exchange method. Appropriate amounts of mixed solution of NaOH (0.3 M), H_3BO_3 (0.1 M), and AgNO_3 (0.2 M) were thoroughly mixed until the initial white color of the solution changed to dark brown. The suspension was then filtrated and washed with deionized water to dissolve any unreacted raw material. Finally, the dark brown powders obtained were dried at 50 °C in air overnight. All the above operations were carried out in darkness.

2.2. Physical Characterization. The crystal structures of as-prepared Ag_2O were determined by glancing angle X-ray diffraction (DX-2007 SSC) with a $\text{Cu K}\alpha$ 40 kV/30 mA X-ray source. The ultraviolet–visible diffuse reflectance spectrum was obtained by using the diffuse reflection method with a Beijing TU-1810 spectrophotometer. The absorption spectrum of MO solution was obtained by using a TU-1901 UV–vis spectrophotometer. The surface morphology was observed with field-emission SEM (JSM-7500F, JEOL). X-ray photoelectron spectroscopy measurements were performed on a VG ESCALAB MKII XPS system with $\text{Al K}\alpha$ source and a charge neutralizer. Electron spin resonance was carried out with an ER200-SRC (Bruker Axs). The photoluminescence spectrum (PL) analysis of Ag_2O was carried out with an FLsp920

instantaneous spectrometer. The COD_{Cr} value of MO solution was determined with a JZ-5B6C water quality analyzer.

2.3. Organic Dye Decomposition. The photoinduced decomposition of the organic dyes was carried out with 0.03 g of Ag_2O powder suspended in a dye solution (16 mg L⁻¹, 10 mL), prepared by dissolving the organic powders in deionized water in a test tube. At room temperature, the test tube was placed on the support standing in the darkroom of an OCRS-IV photoreactor system, which included a 500 W Xe lamp or a 500 W mercury lamp as the artificial light source, a cutoff filter with specified light wavelength, and a water filter. The illumination of different light sources was determined with a TES1335 digital luxmeter. Before illumination, the suspensions were magnetically stirred in the dark for a certain time (usually more than 40 min) to ensure the establishment of an adsorption–desorption equilibrium of dyes on the sample surfaces. After illumination, suspensions including the sample powders and dyes were sampled from the same tube every few seconds. Then the sample powders were separated by centrifuging, and the clarified dye solutions were analyzed with a TU-1901 UV–vis spectrophotometer to determine the concentration of the organic dyes by monitoring the height of the maximum of the absorbance peak in ultraviolet–visible spectra of the solution.

Another contrast sampling method was as follows: eight tubes were employed at the same time, placed in a darkroom placed concentrically around the lamp to conduct the photodecomposition experiment simultaneously, and taken out one-by-one according to the time required for centrifuging and analyzing.

2.4. Density Functional Theory Simulation Conditions. The theoretical calculations were performed using the plane-wave pseudopotential density functional theory (DFT) method. The ion-electron interaction was modeled by ultrasoft pseudopotential in the Vanderbilt form. Valence atomic configurations were $2s^22p^4$ for O and $4d^{10}5s^1$ for Ag. The energy cutoff for a plane wave basis set was 400 eV, and a Monkhorst–Pack k-mesh of $6 \times 6 \times 6$ was used. Geometry optimizations were done before single-point energy calculation, and self-consistent convergence accuracy was set at 1×10^{-6} eV/atom. The convergence criterion for the maximal force between atoms was 0.01 eV. The maximum displacement was 5×10^{-4} Å, and the stress was 60 GPa. The U_p parameter for O was 5 eV, and the U_d parameter for Ag was 11.2 eV. Because of complete symmetry between spin-up and spin-down states, we show only the spin-up results in this paper.

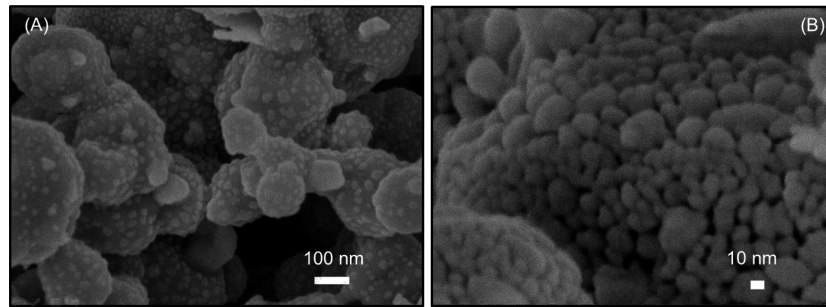


Figure 2. SEM image of Ag_2O sample: (A) 50 000 \times and (B) 300 000 \times .

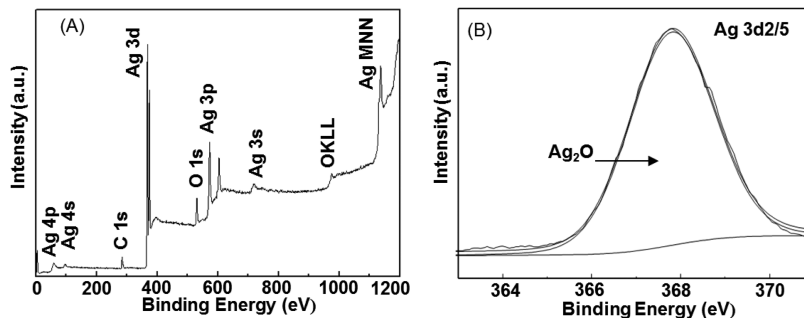


Figure 3. XPS results of fresh Ag_2O sample: (A) full spectrum and (B) $\text{Ag}\ 3\text{d}_{2/5}$ peak.

3. RESULTS AND DISCUSSION

3.1. Characteristics of the As-Prepared Ag_2O Samples.

The silver oxide used in this study was prepared by a facile ion-exchange method with silver nitrate and sodium hydroxide as well as boric acid. The characteristic analysis regarding the structure and components of the as-prepared Ag_2O was carried out before it was used as photocatalyst in the decomposition of the persistent organic pollutant.

3.1.1. Crystal Structure. The appearance of the final product after filtering and drying under the temperature of 50 °C in darkness was black or dark-brown powder (Figure 1).

The crystal structure of the silver oxide was first established as the cubic structure type in 1922 by Niggli.³⁶ The measured lattice constant was 4.728 Å. Later, more accurate crystal structures were established as a result of progress in X-ray diffraction techniques. In 1960, Tadasu Suzuki confirmed the structure of Ag_2O was isostructural with Cu_2O , which was known to be of the cuprite type, and the measured lattice constant of Ag_2O was 4.720 ± 0.004 Å.³⁷ The crystal structure of silver oxide had a cubic symmetry with silver and oxygen atoms in the unit cell. Each oxygen atom was surrounded tetrahedrally by four silver neighbors, while each silver atom had two oxygen neighbors at an equal distance. The XRD patterns of our fresh samples in Figure 1 confirmed this crystal structure, which was pure Ag_2O with cubic structure of the lattice parameter $a = b = c = 4.718$ Å. The calculated crystal grain size of as-prepared Ag_2O was 8.33 nm based on the Debye–Scherrer equation.

3.1.2. Morphology. The results of scanning electron microscopy (SEM) images in Figure 2A showed that the particle size of our sample was between 500 nm and 1 μm, which is consistent with the result of particle size analysis, confirming that the average particle size of sample was 1.0 μm (see Supporting Information, Figure S1), with specific surface area of 0.4726 m² g⁻¹.

However, the SEM images with magnification of 300 000 in Figure 2B confirmed that the Ag_2O particles were not a perfect crystal but an aggregation of plenty of Ag_2O micrograins with a dimension of less than 10 nm, which was consistent with the result of XRD analysis.

3.1.3. Elemental Composition and Valence State. The elemental composition and the valence state of Ag atoms of as-prepared Ag_2O were determined by three analysis methods: energy dispersive spectroscopy (EDS), X-ray fluorescence spectrometer (XRF), and X-ray photoelectron spectroscopy (XPS).

XPS measurements were carried out to determine the existence of B or Na and the valence state of Ag. Results of XPS in Figure 3 confirmed that no heteroatoms such as boron or sodium were introduced in the crystal, although the sample was prepared from the solution containing NaOH and H₃BO₃. The sample was constituted with pure Ag_2O without Ag atoms with other valences. This was consistent with the analysis results of EDS and XRF (see Supporting Information Figures S2 and S3). The testing result of residual liquid after the ion-exchange process with the azomethine-H spectrophotometric method showed that the amount of borate in solution after the ion-exchange process slightly decreased from 0.1 to 0.0912 M (see Supporting Information Method M1). We assumed that it was the adsorption of boric acid on the surface of Ag_2O crystal nucleus that influenced the crystal growth process of silver oxide because boron species could stabilize the nanoparticle size of metal and metal oxide.^{38,39} The boric acid absorbed could be removed in the washing operation of as-prepared samples. Further research about the generating mechanism of such Ag_2O micrograin aggregation was in process.

3.1.4. Energy Band Structure. The band gap energy is a key property influencing the photocatalytic performance of the photocatalyst. The band gap value of Ag_2O was reported to be 1.3 eV⁴⁰ or 1.2 eV.^{41,42} Here, the UV–vis diffusion reflection spectra (UV–vis DRS) of the as-prepared sample in Figure 4

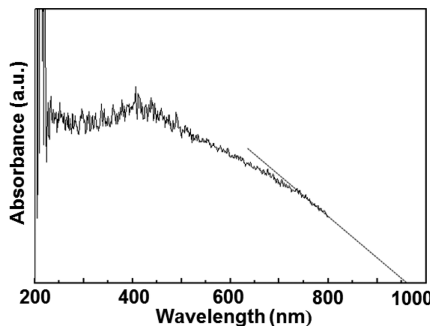


Figure 4. UV-vis DRS of Ag_2O sample from 200 to 800 nm.

was acquired by using a UV-vis spectrophotometer (TU-1901, Ge Beijing Spectrometer, China), and fine BaSO_4 powder was used as a standard. The result showed that the absorbance edge could not be determined directly in the whole measured light region, and there was a strong absorption from 200 to 800 nm. If the tangent line of the absorption curve was extended, the absorption edge could be estimated as 960 nm by the crossing point of tangent line and x -axis. The corresponding band gap value of Ag_2O could be estimated according to the equation⁴³

$$E_g = 1240/\lambda_g \text{ (eV)} \quad (1)$$

where E_g is the band gap of the semiconductor and λ_g is the threshold wavelength, the wavelength of the corresponding absorbance edge. Then the estimated band gap value of Ag_2O was 1.29 eV, which was in agreement with the reported value of 1.3 eV.⁴⁰ Because the absorbance edge of our samples was greater than 800 nm, which entered the spectrum of NIR light, the possibility of photocatalytic activity of Ag_2O in the NIR region was suggested.

3.2. Photocatalytic Performance of Ag_2O . Methyl orange was selected as the target compound for photodecomposition to evaluate the photocatalytic performance of Ag_2O . The corresponding standard absorption curve of MO solution is shown in Supporting Information Figure S4. The light source of OCRS-1 photochemical reactor was a xenon lamp to simulate sunlight, and different optical filters, including visible light (Ultraviolet ZJB380 glass, > 380 nm), red light (Red HB610 glass, > 610 nm), and NIR light (Infrared WHB850 glass, > 850 nm) filters, provided the different light sources (see Supporting Information Figure S5).

3.2.1. Photodecomposition Performance. The adsorption of MO on the surface of Ag_2O and other photocatalysts used as the comparison including Ag_3PO_4 and N-TiO₂ were investigated to exclude the interference of adsorption in determining photocatalytic activity (see Supporting Information Methods M2 and M3). The adsorption equilibrium results confirmed that only 5% of the initial concentration of dye was adsorbed on the surface of Ag_2O after 2 h of sufficient stirring in darkness (see Supporting Information Figure S6). The time required for reaching adsorption equilibrium, 40 min, was far more than that required for the photocatalytic process itself. Therefore, the interference of MO adsorption can be neglected in timing of the fast reaction process.

The pH value of the solution was kept at the value of deionized water during the reaction. To exclude the interference of the self-photodegradation effect of dye under visible light irradiation, experiments of MO illuminated under the same conditions without photocatalyst were carried out (see Supporting Information Figure S7), and results showed

that the self-photodegradation of MO during dye decomposition over Ag_2O could be ignored.

Figure 5 exhibits the fast decomposing rate of MO with as-prepared Ag_2O as photocatalyst under visible light illumination

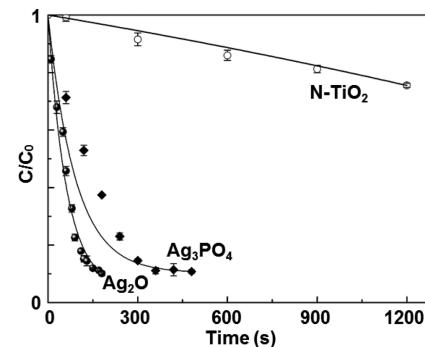


Figure 5. Photocatalytic activity of homemade Ag_2O , Ag_3PO_4 , and N-TiO₂.

with light illumination of 16.35 kLux. The other two curves are the MO decomposition process photocatalyzed by homemade Ag_3PO_4 and N-doped TiO₂ with the same mass (0.03 g). Results showed that the dye could be eliminated completely within 120 s by Ag_2O , which was far faster than other two. The comparison of MO decomposition rates photocatalyzed by three photocatalysts with the same specific area (0.05 m^2) and of the same metal atomicity (0.26 mmol) are shown in Supporting Information Figures S8 and S9, which also confirmed the ultrafast MO degradation rate photocatalyzed by Ag_2O when driven by visible light.

Figure 6 exhibits the photocatalytic activity of Ag_2O under different light sources. Results showed that the as-prepared

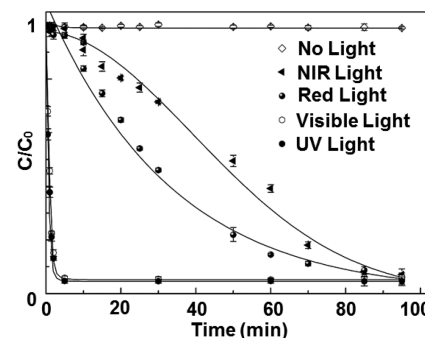


Figure 6. Photocatalytic activity of Ag_2O with different light sources.

Ag_2O samples could function not only in the traditional spectrum range such as UV or visible light but also in the wider spectrum with long wavelength, i.e., red light (wavelength > 610 nm) or NIR light (wavelength > 850 nm). However, the MO degradation rate under red light or NIR light irradiation decreased sharply from 120 s to about 2 h. Such sharp decrease of photocatalytic performance of Ag_2O should be ascribed to the reduction of red light or NIR light illumination (red light is 0.18 kLux, and NIR light is 0.06 kLux) and the decrease of photocatalytic activity of Ag_2O under the spectrum with longer wavelength, simultaneously.

3.2.2. Photodegradation Products of MO with Ag_2O . Although the color removal of MO with Ag_2O was almost completed in 120 s under visible light irradiation because the

chromophoric groups of dye were damaged, it does not mean that the total organic ingredients and structure of pollutant has been damaged for the purpose of environmental protection. It is necessary to verify whether all the organic pollutant has been mineralized completely into CO_2 and other inorganic materials. Therefore, the chemical oxygen demand (COD) value of MO solution before and after photodecomposition was determined with a strong oxidant, potassium dichromate, which then was marked as COD_{Cr} , to confirm the actual mineralization effect of organic pollutant in the photocatalysis process. The COD removal ratio was calculated and is shown in Figure 7. The

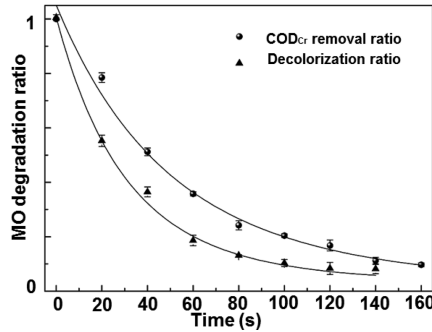


Figure 7. COD_{Cr} change of MO solution in photodegradation process with Ag₂O.

results confirmed that the COD_{Cr} of MO solution during the photodecomposition period decreased sharply and was completed after 160 s, although the decreasing rate of COD_{Cr} was lower than the decolorization rate. However, the remaining COD_{Cr} of degraded MO solution confirmed that there were some small organic compound residues in solution, although most of the MO was mineralized into CO₂ and water.

The MO solution samples with different photodecomposition times were taken out and analyzed with UV-vis spectrum. The full UV-vis spectrum of MO solution is shown in Figure 8. The typical absorption peak of MO solution at 465 nm, the

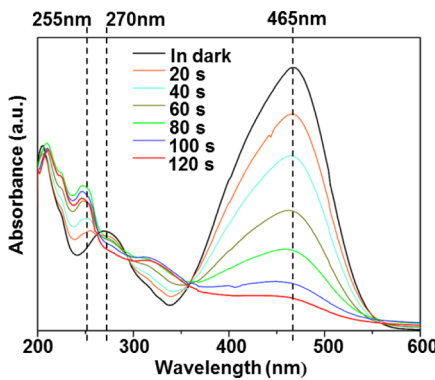


Figure 8. UV-vis spectrum of MO solution in photodegradation process.

azo structure, decreased sharply, which confirmed that the chromophoric group of MO was destroyed completely. The absorption peak at 270 nm of the benzene ring conjugate structure was also weakened at the same time. However, a new peak at 255 nm emerged after the beginning of the photodecomposition process, reaching the peak value after 80 s, and commencing to fade after this extreme point. This new peak should be ascribed to an intermediate judged to be a kind

of substituted benzene. This organic intermediate also was decomposed in a sequent photodegradation process. This result confirmed that Ag₂O was a strong photocatalyst, mineralizing MO completely in 120 s.

3.2.3. Stability. Stability of as-prepared Ag₂O was investigated with three methods: repeated use of the same sample and exposure of the sample under sunlight in air and in water. The times required for reaching 90% MO conversion are presented in Figure 9 to evaluate the decaying of photocatalytic

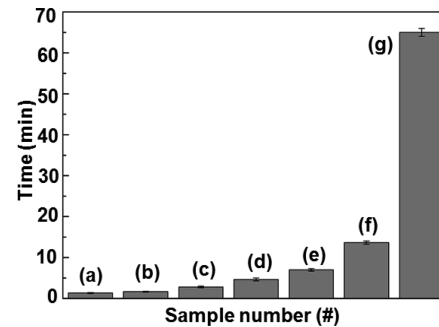


Figure 9. Reacting time for reaching 90% MO degradation rate with different samples: (a) fresh sample, (b) 3-cycle sample, (c) 8-cycle sample, (d) 24 h exposed sample under sunlight in air, (e) 24 h exposed sample under sunlight in water, (f) fresh Ag₃PO₄, and (g) fresh N-TiO₂.

activity. Results suggested that reusing and exposure of Ag₂O resulted in only slight performance degradation. The Ag₂O sample used after 8 cycles or exposed after 24 h decomposed MO completely within 6 and 8 min, respectively. Such performance after decaying was still better than that of fresh Ag₃PO₄ or N-TiO₂.

XRD and XPS analyses of used and exposed Ag₂O were carried out to investigate the slight performance degradation of Ag₂O. The XRD peaks of used Ag₂O sample in Figure 10 after

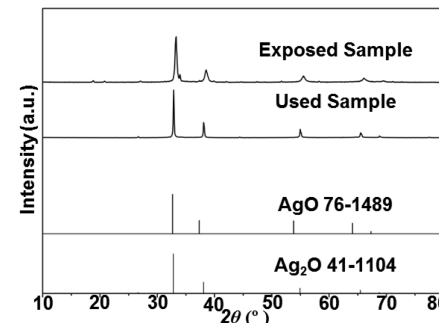


Figure 10. XRD of used and exposed Ag₂O samples.

eight cycles were a little narrower and higher than those of the fresh sample, which showed the increasing tendency of crystallinity of Ag₂O. The calculated crystal grain size increased to 15.87 nm. The decrease of surface area and active sites of perfect Ag₂O crystal could evoke the performance degradation. Such growth of Ag₂O crystal grains also was observed in the SEM results of the exposed sample (Figure 11).

XPS results of the exposed sample (see Supporting Information Figure S10) confirmed that no obvious decomposition of Ag₂O was observed, and the exposed Ag₂O sample still consisted of pure Ag₂O. This result excluded the possibility

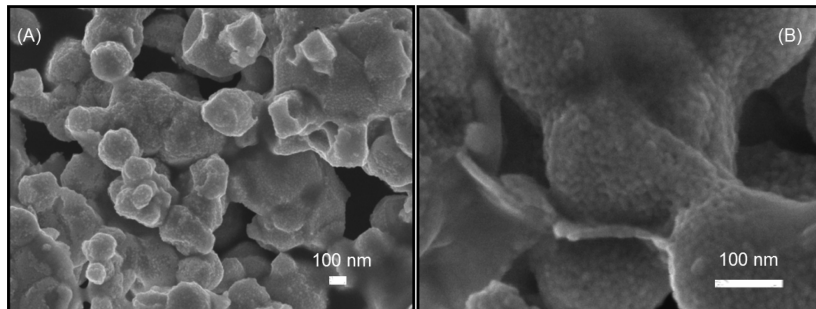


Figure 11. SEM of exposed Ag_2O samples: (A) 50 000 \times ; (B) 200 000 \times .

that the Ag_2O decomposition caused the performance degradation of Ag_2O after long exposure times.

3.2.4. Performance under Sunlight. The performance of Ag_2O working with natural sunlight under varied weather conditions, such as sunny, overcast, cloudy, rainy, morning, noon, and evening, was investigated, and the results are presented in Figure 12. The actual experimental process under

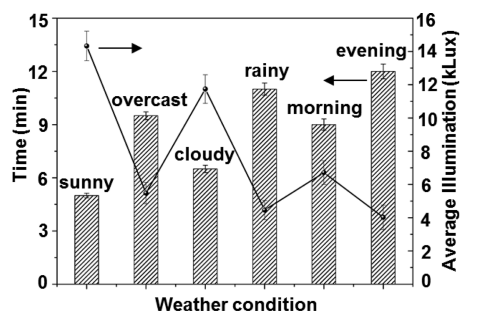


Figure 12. Degradation time of MO with Ag_2O under various weather conditions.

sunny conditions was recorded on video and is provided as Supporting Information Video V1. Results showed that the MO degradation rate fluctuated little, which verified the steady performance and promising practical application prospects of Ag_2O . Furthermore, the photocatalytic process of MO with Ag_2O under irradiation of red light or NIR contained in sunlight was investigated by employing an optical filter to block undesired light (see Supporting Information Method M4). The results presented in Supporting Information Figure S11 show that the dye was eliminated within 24 or 40 min under illumination of solar red light or NIR, respectively. This also verified that the photocatalytic performance of Ag_2O driven by red/NIR light was enhanced with the increase of light intensity (average illumination of solar red light is 0.38 kLux, and that of NIR light is 0.12 kLux).

In addition, the photocatalytic decomposition of other typical organic pollutants, such as phenol, methylene blue, cyanuramide, and acid fuchsine, with Ag_2O under solar light was carried out to confirm the wide applicability of Ag_2O as photocatalysts. The details of experiments and results are shown in Supporting Information Figure S12. The results confirmed that all of the above organic compounds can be degraded in less than 10 min, which demonstrated the superb photocatalytic performance and wide applied scope of Ag_2O .

3.3. Photocatalytic Mechanism of Ag_2O . It is known that superoxide anion radicals, $\cdot\text{OH}$ radicals, and photo-generated holes are common possible active species in photocatalytic degradation of organic pollutants.¹ However,

because the electrode potential of $\cdot\text{OH}$ is 2.80 eV and the band gap of Ag_2O is 1.3 eV, they should be excluded as possible active species for as-prepared Ag_2O samples. It is necessary to explore the role of Ag_2O in the photocatalytic process, find the possible active species, and establish its working mechanism.

3.3.1. Determination of Radical Species. Here, electron spin resonance with an ER200-SRC instrument was employed to investigate the active species, and 5,5-dimethyl-1-pyrroline-N-oxide (DMPO) was used for the spin trap. The results shown in Figure 13 confirmed no such radicals were generated

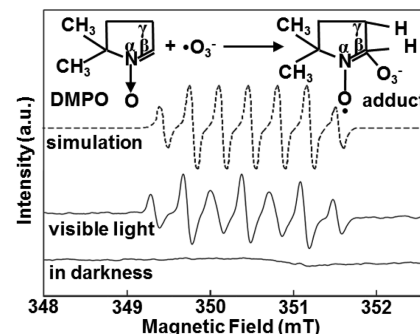


Figure 13. ESR signals of Ag_2O and the simulation curve of ozone anion radical DMPO- $\cdot\text{O}_3^-$ with WINEPR Simfonia.

in water under light illumination. The signal observed under visible light illumination was distinct from that of DMPO- $\cdot\text{OH}$, DMPO- $\cdot\text{O}_2^-$, as well as their overlap. Because the signal was a seven line-spectra with ESR hyperfine splitting constant g of 2.0064 and a_{N} , $a_{\text{H}\beta}$, and $a_{\text{H}\gamma}$ of 0.375 mT, it was judged to be DMPO- $\cdot\text{O}_3^-$, which could be named as ozone anion radicals.⁴⁴ This could be attributed to the stronger electronegativity of O^{3-} than $\cdot\text{OH}$ and O^{2-} , which caused the equivalent splitting of the H proton at α , β , and γ positions, generating 12 peaks according to the equation $\Pi(2n_i I_i + 1)$. Because of the overlapping of 10 peaks, a septet peak group with an intensity ratio of 1:2:2:2:2:1 was shown.

Because only radical $\cdot\text{O}_3^-$ was observed in solution with Ag_2O under light irradiation, it could be judged as the highly probable active species in the photocatalytic process of Ag_2O . The slight weakening of ESR signal intensity of used Ag_2O sample also confirmed the possible relationship between the photocatalytic performance and generated $\cdot\text{O}_3^-$ concentration (see Supporting Information Figure S13). It has been suggested that $\cdot\text{O}_3^-$ could be formed by two possible routes: the reaction of dissolved O_2 with the hole center O^- generated from the lattice oxygen O^{2-} oxidized with the photogenerated hole⁴⁵ or reaction of O_3 with the photogenerated electrons.⁴⁶ The ozone

anion radical was an extremely reactive species and should oxidize organics very quickly.⁴⁷

3.3.2. Radical-Trapping Experiments. To identify the major active species in the degradation of MO on the surface of Ag₂O and to determine the formation route of ·O³⁻, radical-trapping experiments were conducted with four chemicals: benzoquinone (a superoxide anion radical scavenger), methanol (a hole scavenger), *tert*-butanol (a ·OH radical scavenger), and indigo carmine (an ozone scavenger). The spectra of different mixtures composed with MO and a certain scavenger are shown in Supporting Information Figure S14, which confirmed that there was no masking effect of selected scavenger for MO detection process. The MO degradation curve in Figure 14

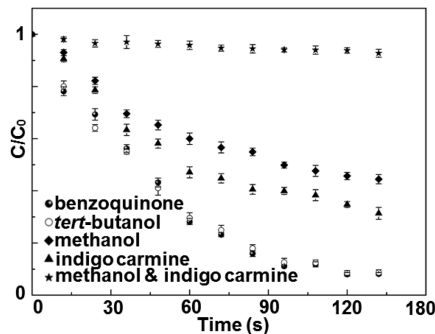


Figure 14. Photocatalytic activities of Ag₂O in the presence of different scavengers.

showed that the addition of methanol or indigo carmine degraded the photocatalytic activity of Ag₂O significantly. With the simultaneous addition of methanol and indigo carmine, the photodegradation process of MO with Ag₂O as photocatalyst was stopped. This confirmed that it was a combined function of photogenerated holes and ozone anion radicals under visible light irradiation that dominated the reaction process of oxidative degradation of MO. This supposed mechanism of Ag₂O differs from the traditional photo-oxidized route of TiO₂.

3.3.3. Redox Potential. In general, the photocatalytic activity of a photocatalyst is determined by the band gap, the oxidation potential of photogenerated holes, and the separation efficiency of photogenerated electrons and holes. Ag₂O can harvest visible and NIR light because of the small band gap (1.29 eV). To investigate the oxidation potential of photogenerated holes, the conduction band (CB) and valence band (VB) potentials to²⁷ Ag₂O at the point of zero charge can be calculated by

$$E_{VB} = X - E_e + 0.5E_g \quad (2)$$

where X is the Pearson absolute electronegativity of the semiconductor, which is defined as the geometric mean of the absolute electronegativity of the constituent atoms,⁴⁸ and E_e is the energy of free electrons on the hydrogen scale (ca. 4.69 eV);⁴¹ E_{VB} is the VB edge potential, and E_g is the band gap of the semiconductor. The conduction band (CB) position can be determined by

$$E_{CB} = E_{VB} - E_g \quad (3)$$

The X value for Ag₂O is ca. 5.29 eV.⁴¹ On the basis of the above equations, the top of the VB and the bottom of the CB of Ag₂O are calculated to be 1.25 and -0.04 eV, respectively. The results in Figure 15 indicate that the oxidation potential of photogenerated holes of Ag₂O is high enough to generate ozone because the electrode potential of O₃/O₂ in neutral

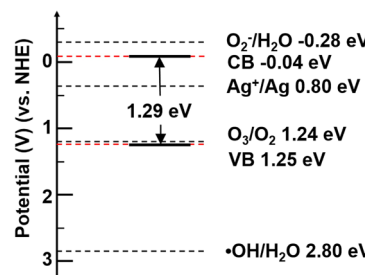


Figure 15. Diagram for band energy of Ag₂O and schematic drawing of redox potentials of Ag₂O.

solution is 1.24 eV, lower than that for generating ·OH radical with electrode potential of 2.80 eV and superoxide anion radical with electrode potential of -0.28 eV.

When the redox potential result is combined with the XPS results, which revealed no significant decomposition of Ag₂O and hence no significant oxidation of lattice oxygen O²⁻, and with the fact that the formation of ·O³⁻ can be interrupted by adding the ozone scavenger, it can be inferred that the formation of ·O³⁻ should be in accordance with the following reactions: the dissolved oxygen reacted with the photogenerated hole and hydroxyl ion in aqueous solution to form ozone and forms the ozone anion radical after accepting the photogenerated electrons. This also can explain the excellent stability of Ag₂O because the photogenerated holes and electrons were consumed, preventing carrier recombination in photocatalysis. The produced radical, ·O³⁻, a strong oxidizer, can oxidize the organic pollutants with a relatively long lifetime, working together and reinforcing the decomposition performance of photogenerated holes of Ag₂O.

3.3.4. DFT Simulation. To obtain further insight into the electronic structure and chemical bonding mechanism of prepared Ag₂O, ab initio density functional theory calculations have been carried out. The band gap from DFT calculations often provides important insight into the physicochemical behavior of the investigated materials in spite of its underestimation. Calculated band gap energy was reported as 0.40 eV⁴⁹ or 0.88 eV;⁵⁰ no band gap has even been reported.⁵¹ Here, the crystal cell parameters were input based on the XRD results of as-prepared Ag₂O (see Supporting Information Figure S15), and the calculated band structure is presented in Figure 16. It was noted that Ag₂O was a semiconductor with a direct band gap at the G point. The calculated band gap for Ag₂O was 1.236 eV, which was a little smaller than the experimental value of 1.29 eV obtained or 1.3 eV reported.^{38,40,48} This slight discrepancy could be ascribed to the underestimation of the DFT, which considered only excited states in the calculation.

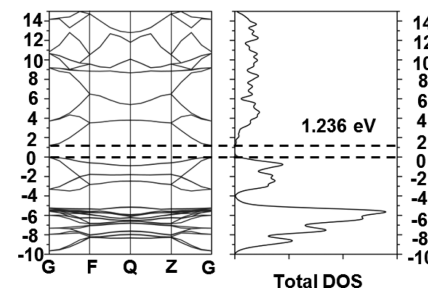


Figure 16. Energy band diagram and total density of states for Ag₂O calculated by a density functional method.

The calculated total density of states (TDOS) and partial density of states (PDOS) for Ag_2O is plotted in Figure 16 and Supporting Information Figure S16, respectively. The valence band of Ag_2O clearly split into two regions. The lower region has the $\text{O}^{2\text{p}}$ features, whereas the upper region is dominated by $\text{Ag}^{5\text{d}}$ states. It is noteworthy that $\text{Ag}^{5\text{s},5\text{p}}$ states exhibition-vanishing distributions within the valence band have an intraatomic hybridization of $\text{Ag}^{5\text{d}}$ states with $\text{Ag}^{5\text{s},5\text{p}}$ states. For Ag_2O , the width of the valence band is equal to 10 eV. The $\text{Ag}^{5\text{d}}$ states have an intensity peak at -5.57 eV. In the lower region, two $\text{O}^{2\text{p}}$ maxima are found at -8.52 and -0.58 eV.

3.3.5. Influence of Aggregation Structure. Another possibly important reason for the superb performance and high stability of our as-prepared samples is the strong quantum confinement effect of Ag_2O . The diminutive size, massive specific area, and numerous crystal boundaries supplied by Ag_2O not only increase the probability of recombination of photogenerated hole and electron at the surface of crystal but also provide high escape probability of photogenerated electrons and exposure probability of photogenerated holes on the surface. The high contact probability of the hole with dye and oxygen, or electron with ozone, is beneficial for the oxidation process, sharply decreasing the reduction probability of Ag^+ ion and oxidation probability of lattice O^{2-} , simultaneously.

As is well-known, tiny semiconductor microcrystals can be classified as quantum dots (QDs) when the particle size is less than 100 nm and consequently shows strong quantum confinement effect and releases fluorescent light after light irradiation. This presumption was supported by the photoluminescence (PL) spectrum analysis of as-prepared and commercial Ag_2O samples in Figure 17. The PL analysis

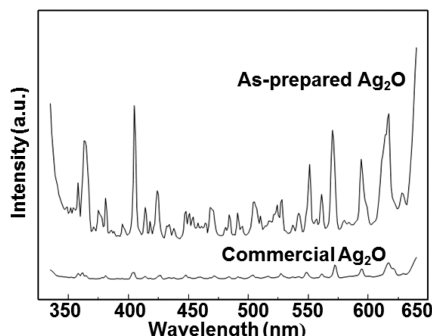


Figure 17. Photoluminescence spectra from 300 to 650 nm of as-prepared Ag_2O sample with that of commercial Ag_2O powder as contrast.

results showed that our samples generated strong fluorescent light spanning the whole visible light range from 335 to 780 nm, which meant high recombination rate of photogenerated holes and electrons at the surface of Ag_2O QDs. The strength of fluorescent light was much greater than that of the commercial Ag_2O . It is reasonably assumed that more grain boundaries of QDs can supply a higher surface area and enhance photogenerated electrons escape probability, consequently strengthening the photocatalytic activity.

The construction of this aggregation of Ag_2O QDs could be ascribed to the introduction of boric acid in the preparation process. Other alternatives such as pure NaOH, NaOH + H_2SiO_3 , KOH + H_3BO_3 , and $\text{Na}_2\text{B}_4\text{O}_7$ were attempted to prepare Ag_2O with the same procedure. Results (see Supporting Information Figures S17 and S18) showed that

only the sample prepared with KOH + H_3BO_3 had the similar structure and almost the same photocatalytic performance as that of the as-prepared sample with NaOH + H_3BO_3 , which confirmed that it was the addition of H_3BO_3 that helped the construction of the microstructure of Ag_2O QDs, strengthening the photocatalytic performance of Ag_2O .

3.3.6. Photocatalytic Process Mechanism. On the basis of the above analysis, the working mechanism of Ag_2O is conjectured and described in Figure 18. The Ag_2O QDs

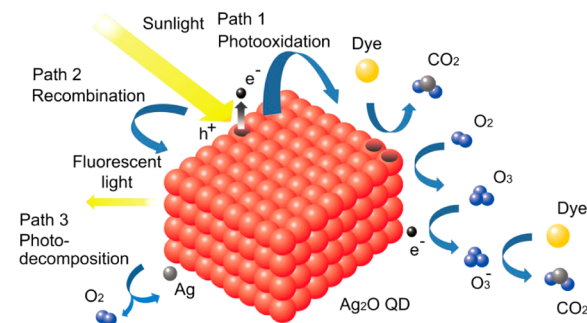
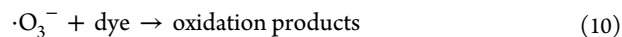
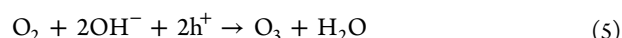


Figure 18. Diagram of Ag_2O photocatalysis process with different paths.

aggregate together, not amalgamate, to form bigger particles with numerous crystal boundaries and high surface area. Under the illumination of UV light, visible light, or red/NIR light, the electrons of Ag_2O are transmitted from the valence band to the conduction band, leaving the hole in the valence band (eq 4). The photogenerated holes and electrons could induce three reaction paths: recombining with each other, reacting inside with lattice Ag^+ and O^{2-} , and reacting outside with the materials to complete the photocatalytic process.

Specifically, the photogenerated holes could induce four reactions. First, the holes can convert the dissolved oxygen in the solution to ozone (eq 5). Second, the holes react with dye to photo-oxidize and mineralize it directly (eq 6). Third, the holes can recombine with photogenerated electrons, lowering the quantum efficiency of Ag_2O (eq 7). Fourth, the holes could oxidize the lattice O^{2-} in Ag_2O , releasing oxygen and destroying the stability of Ag_2O (eq 8).³³ The photogenerated electrons also could induce three reactions. First, it can be captured by ozone to form ozone anion radicals, oxidizing the dye (eqs 9 and 10). Second, it reacts with lattice Ag^+ to generate metallic Ag, decaying the photocatalytic performance of Ag_2O (eq 11). Last, it could recombine with photogenerated holes (eq 7).



Because the as-prepared Ag_2O sample is an aggregation of Ag_2O QDs, which can provide numerous crystal boundary and high surface area for escaping of photogeneration electrons and contacting of photogeneration holes with external materials, the competition of the third reaction path should be higher than that of the former two. Thus, the photocatalytic performance and stability of Ag_2O prepared is upgraded significantly.

4. CONCLUSION

We have successfully prepared novel Ag_2O photocatalyst working under UV, visible light, and red/NIR light irradiation with a facile precipitation method. Methyl orange can be degraded completely with the help of Ag_2O under UV or visible light irradiation in 120 s. If driven by red or NIR light, the decomposition of MO can be completed within 2 h, or even within 40 min under solar red/NIR light. This superb photo-oxidation performance of Ag_2O is kept almost essentially constant after repeated use or exposure in sunlight. Such high efficiency and stability of Ag_2O should be attributed to the narrow band gap of Ag_2O , 1.29 eV, and high surface area and numerous crystal boundaries supplied by Ag_2O QDs. The photogenerated holes and ozone anion radicals generated after various light illuminations are the active species for the photo-oxidation process of Ag_2O . We believe this novel photocatalyst with amazing performance possesses promising prospects for future application.

■ ASSOCIATED CONTENT

Supporting Information

Particle size distribution of as-prepared Ag_2O sample; EDS and XRF analysis results of Ag_2O ; standard spectrum of methyl orange solution; wavelength spectrum of a 500 W Xe lamp and a 500 W mercury lamp with different optical filters; adsorption of MO on the surface of Ag_2O and other photocatalysts; MO degradation curve without any photocatalyst; photocatalytic activity of Ag_2O , Ag_3PO_4 , and N-TiO₂ with same surface area and same metal atomicity; XPS results of exposed Ag_2O sample; photocatalytic activity of Ag_2O under solar red light and NIR; photocatalytic decomposition of different organic pollutants with Ag_2O under solar light irradiation; ESR signals of Ag_2O under different conditions; spectrophotometer spectra of solutions of MO with different scavengers; Ag_2O crystal cell model before and after relaxation for DFT simulation; calculated PDOS for Ag_2O ; SEM graphics of Ag_2O produced with varied acid or base; photocatalytic performance of Ag_2O with different preparation procedures; determination program of boron concentration in solution; preparation program of N-TiO₂ and Ag_3PO_4 ; experimental process of MO photodegradation with Ag_2O under irradiation of solar red light or NIR; and video of MO quick photodegradation process with Ag_2O under natural sunlight irradiation. This material is available free of charge via the Internet at <http://pubs.acs.org>.

■ AUTHOR INFORMATION

Corresponding Author

*Tel.: +86-28-85990133. Fax: +86-28-85460556. E-mail: weijiang@scu.edu.cn.

Notes

The authors declare no competing financial interest.

■ ACKNOWLEDGMENTS

We appreciated the financial support from the National Natural Science Foundation of China project (21176157, 21476146, and Key Project 21236004).

■ REFERENCES

- (1) Loannis, K.; Triantafyllos, A. TiO₂-assisted photocatalytic degradation of azo dyes in aqueous solution: Kinetic and mechanistic investigations. *Appl. Catal., B* **2004**, *49*, 1.
- (2) Fujishima, A.; Honda, K. Electrochemical photolysis of water at a semiconductor electrode. *Nature* **1972**, *238*, 37.
- (3) Frank, S.; Bard, A. Heterogeneous photocatalytic oxidation of cyanide ion in aqueous solutions at titanium dioxide powder. *J. Am. Chem. Soc.* **1977**, *99*, 303.
- (4) Chong, M. N.; Jin, B.; Chow, C. W.; Saint, C. Recent developments in photocatalytic water treatment technology: A review. *Water Res.* **2010**, *44*, 2997.
- (5) Pelaez, M.; Nolan, N. T.; Pillai, S. C.; Seery, M. K.; Falaras, P.; Kontos, A. G.; Dunlop, P. S.; Hamilton, J. W.; Byrne, J. A.; O'Shea, K. A review on the visible light active titanium dioxide photocatalysts for environmental applications. *Appl. Catal., B* **2012**, *125*, 331.
- (6) Fujishima, A.; Rao, T.; Tryk, D. Titanium dioxide photocatalysis. *J. Photochem. Photobiol., C* **2000**, *1*, 1.
- (7) Fujishima, A.; Zhang, X.; Tryk, D. Heterogeneous photocatalysis: From water photolysis to applications in environmental cleanup. *Int. J. Hydrogen Energy* **2007**, *32*, 2664.
- (8) Kabra, K.; Chaudhary, R.; Sawhney, R. L. Treatment of hazardous organic and inorganic compounds through aqueous-phase photocatalysis: A review. *Ind. Eng. Chem. Res.* **2004**, *43*, 7683.
- (9) Park, H.; Park, Y.; Kim, W.; Choi, W. Surface modification of TiO₂ photocatalyst for environmental applications. *J. Photochem. Photobiol., C* **2013**, *15*, 1.
- (10) Akpan, U. G.; Hameed, B. H. Parameters affecting the photocatalytic degradation of dyes using TiO₂-based photocatalysts: A review. *J. Hazard. Mater.* **2009**, *170*, 520.
- (11) Daghrir, R.; Drogui, P.; Robert, D. Modified TiO₂ for environmental photocatalytic applications: A review. *Ind. Eng. Chem. Res.* **2013**, *52*, 3581.
- (12) Ochiai, T.; Fujishima, A. Photoelectrochemical properties of TiO₂ photocatalyst and its applications for environmental purification. *J. Photochem. Photobiol., C* **2012**, *13*, 247.
- (13) Chatterjee, D.; Dasgupta, S. Visible light induced photocatalytic degradation of organic pollutants. *J. Photochem. Photobiol., C* **2005**, *6*, 186.
- (14) Rehman, S.; Ullah, R.; Butt, A. M.; Gohar, N. D. Strategies of making TiO₂ and ZnO visible light active. *J. Hazard. Mater.* **2009**, *170*, 560.
- (15) Ibadon, A.; Fitzpatrick, P. Heterogeneous Photocatalysis: Recent Advances and Applications. *Catalysts* **2013**, *3*, 189.
- (16) Pei, D.; Luan, J. Development of Visible Light-Responsive Sensitized Photocatalysts. *Int. J. Photoenergy* **2012**, *2012*, 1.
- (17) Asahi, R.; Morikawa, T.; Ohwaki, T.; Aoki, K.; Taga, Y. Visible-light photocatalysis in nitrogen-doped titanium oxides. *Science* **2001**, *293*, 269.
- (18) Nakamura, R.; Tanaka, T.; Nakato, Y. Mechanism for visible light responses in anodic photocurrents at N-doped TiO₂ film electrodes. *J. Phys. Chem. B* **2004**, *108*, 10617.
- (19) Mrowetz, M.; Balcerksi, W.; Colussi, A.; Hoffmann, M. R. Oxidative power of nitrogen-doped TiO₂ photocatalysts under visible illumination. *J. Phys. Chem. B* **2004**, *108*, 17269.
- (20) Zhang, X.; Ai, Z.; Jia, F.; Zhang, L.; Fan, X.; Zou, Z. Selective synthesis and visible-light photocatalytic activities of BiVO₄ with different crystalline phases. *Mater. Chem. Phys.* **2007**, *103*, 162.
- (21) Li, G.; Zhang, D.; Yu, J. C. Ordered mesoporous BiVO₄ through nanocasting: A superior visible light-driven photocatalyst. *Chem. Mater.* **2008**, *20*, 3983.

- (22) Tokunaga, S.; Kato, H.; Kudo, A. Selective preparation of monoclinic and tetragonal BiVO_4 with scheelite structure and their photocatalytic properties. *Chem. Mater.* **2001**, *13*, 4624.
- (23) Yi, Z.; Ye, J.; Kikugawa, N.; Kako, T.; Ouyang, S.; Stuart-Williams, H.; Yang, H.; Cao, J.; Luo, W.; Li, Z. An orthophosphate semiconductor with photooxidation properties under visible-light irradiation. *Nat. Mater.* **2010**, *9*, 559.
- (24) Tang, J.; Liu, Y.; Li, H.; Tan, Z.; Li, D. A novel Ag_3AsO_4 visible-light-responsive photocatalyst: Facile synthesis and exceptional photocatalytic performance. *Chem. Commun. (Cambridge, U.K.)* **2013**, *49*, 5498.
- (25) Liu, X.; Hu, J.; Li, J.; Hu, Y.; Shao, Y.; Yang, H.; Tong, G.; Qian, H. Facile synthesis of $\text{Ag}_2\text{WO}_4/\text{AgCl}$ nanorods for excellent photocatalytic properties. *Mater. Lett.* **2013**, *91*, 129.
- (26) Hu, X.; Hu, C. Preparation and visible-light photocatalytic activity of Ag_3VO_4 powders. *J. Solid State Chem.* **2007**, *180*, 725.
- (27) Dai, G.; Yu, J.; Liu, G. A New Approach for Photocorrosion Inhibition of Ag_2CO_3 Photocatalyst with Highly Visible-Light-Responsive Reactivity. *J. Phys. Chem. C* **2012**, *116*, 15519.
- (28) Singh, J.; Uma, S. Efficient photocatalytic degradation of organic compounds by ilmenite AgSbO_3 under visible and UV light irradiation. *J. Phys. Chem. C* **2009**, *113*, 12483.
- (29) Ouyang, S.; Kikugawa, N.; Chen, D.; Zou, Z.; Ye, J. A systematical study on photocatalytic properties of AgMO_2 ($\text{M} = \text{Al}, \text{Ga}, \text{In}$): Effects of chemical compositions, crystal structures, and electronic structures. *J. Phys. Chem. C* **2009**, *113*, 1560.
- (30) Wang, P.; Huang, B.; Qin, X.; Zhang, X.; Dai, Y.; Wei, J.; Whangbo, M. H. Ag@AgCl: A highly efficient and stable photocatalyst active under visible light. *Angew. Chem., Int. Ed.* **2008**, *47*, 7931.
- (31) Qin, W.; Zhang, D.; Zhao, D.; Wang, L.; Zheng, K. Near-infrared photocatalysis based on $\text{YF}_3:\text{Yb}^{3+}\text{Tm}^{3+}/\text{TiO}_2$ core/shell nanoparticles. *Chem. Commun. (Cambridge, U.K.)* **2010**, *46*, 2304.
- (32) Wang, G.; Huang, B.; Ma, X.; Wang, Z.; Qin, X.; Zhang, X.; Dai, Y.; Whangbo, M. H. $\text{Cu}_2(\text{OH})\text{PO}_4$, a near-infrared-activated photocatalyst. *Angew. Chem., Int. Ed.* **2013**, *52*, 4810.
- (33) Mor, G. K.; Kim, S.; Paulose, M.; Varghese, O. K.; Shankar, K.; Basham, J.; Grimes, C. A. Visible to near-infrared light harvesting in TiO_2 nanotube array–P3HT based hetero junction solar cells. *Nano Lett.* **2009**, *9*, 4250.
- (34) Wang, X.; Li, S.; Yu, H.; Yu, J.; Liu, S. Ag_2O as a new visible-light photocatalyst: Self-stability and high photocatalytic activity. *Chem.—Eur. J.* **2011**, *17*, 7777.
- (35) Wang, G.; Ma, X.; Huang, B.; Cheng, H.; Wang, Z.; Zhan, J.; Qin, X.; Zhang, X.; Dai, Y. Controlled synthesis of Ag_2O microcrystals with facet-dependent photocatalytic activities. *J. Mater. Chem.* **2012**, *22*, 21189.
- (36) Niggli, P. Die Kristallstruktur einiger Oxyde I. *Z. Kristallogr., Kristallgeom., Kristallphys., Kristallchem.* **1922**, *57*, 253.
- (37) Suzuki, T. X-Ray Study on the Binding Properties of Cu_2O and Ag_2O Crystals. *J. Phys. Soc. Jpn.* **1960**, *15*, 2018.
- (38) Yin, A.; Qu, J.; Guo, X.; Dai, W.-L.; Fan, K. The influence of B-doping on the catalytic performance of Cu/HMS catalyst for the hydrogenation of dimethyloxalate. *Appl. Catal., A* **2011**, *400*, 39.
- (39) Zhao, S.; Yue, H.; Zhao, Y.; Wang, B.; Geng, Y.; Lv, J.; Wang, S.; Gong, J.; Ma, X. Chemoselective synthesis of ethanol via hydrogenation of dimethyl oxalate on Cu/SiO_2 : Enhanced stability with boron dopant. *J. Catal.* **2013**, *297*, 142.
- (40) Tjeng, L.; Meinders, M.; van Elp, J.; Ghijssen, J.; Sawatzky, G.; Johnson, R. Electronic structure of Ag_2O . *Phys. Rev. B: Condens. Matter Mater. Phys.* **1990**, *41*, 3190.
- (41) Xu, Y.; Schoonen, M. A. The absolute energy positions of conduction and valence bands of selected semiconducting minerals. *Am. Mineral.* **2000**, *85*, 543.
- (42) Fortin, E.; Weichman, F. Photoconductivity in Ag_2O . *Phys. Status Solidi B* **1964**, *5*, 515.
- (43) Bird, J. P. *Electron Transport in Quantum Dots*; Kluwer Academic Publishers: Boston, 2003.
- (44) Ye, M.; Chen, Z.; Shen, J.; Ben, Y.; Liu, X. ESR Analysis on the Ozone Enhanced Photocatalytic Activity of Aqueous Nanosized Titanium Dioxide Suspensions. *Imaging Sci. Photochem.* **2008**, *26*, 460.
- (45) Einaga, H.; Ogata, A.; Futamura, S.; Ibusuki, T. The stabilization of active oxygen species by Pt supported on TiO_2 . *Chem. Phys. Lett.* **2001**, *338*, 303.
- (46) Ochiai, T.; Nanba, H.; Nakagawa, T.; Masuko, K.; Nakata, K.; Murakami, T.; Nakano, R.; Hara, M.; Koide, Y.; Suzuki, T.; Ikekita, M.; Morito, Y.; Fujishima, A. Development of an O_3 -assisted photocatalytic water-purification unit by using a TiO_2 modified titanium mesh filter. *Catal. Sci. Technol.* **2011**, *2*, 76.
- (47) Todres, Z. V. *Ion-Radical Organic Chemistry: Principles and Applications*; Taylor & Francis: Boca Raton, FL, 2002.
- (48) Pearson, R. G. Absolute electronegativity and hardness correlated with molecular orbital theory. *Proc. Natl. Acad. Sci. U.S.A.* **1986**, *83*, 8440.
- (49) Czyrk, M.; de Groot, R.; Dalba, G.; Fornasini, P.; Kisiel, A.; Rocca, F.; Burattini, E. Ag_2O band structure and X-ray-absorption near-edge spectra. *Phys. Rev. B: Condens. Matter Mater. Phys.* **1989**, *39*, 9831.
- (50) Gordienko, A. B.; Zhuravlev, Y. N.; Fedorov, D. G. Band structure and chemical bonding in Cu_2O and Ag_2O oxides. *Phys. Solid State* **2007**, *49*, 223.
- (51) Deb, A.; Chatterjee, A. K. The electronic structure and chemical bonding mechanism of silver oxide. *J. Phys.: Condens. Matter* **1998**, *10*, 11719.